INSTITUTE OF PHYSICS PUBLISHING JOURNAL OF OPTICS A: PURE AND APPLIED OPTICS

J. Opt. A: Pure Appl. Opt. **6** (2004) 569–584 PII: S1464-4258(04)73241-9

Nonlinear frequency conversion in semiconductor optical waveguides using birefringent, modal and quasi-phase-matching techniques

S Venugopal Rao, K Moutzouris and M Ebrahimzadeh[1]

School of Physics and Astronomy, University of St Andrews, North Haugh, Fife KY16 9SS, UK

E-mail: vrs2@st-and.ac.uk and me@st-and.ac.uk

Received 1 December 2003, accepted for publication 18 March 2004
Published 23 April 2004
Online at stacks.iop.org/JOptA/6/569
DOI: 10.1088/1464-4258/6/6/013

Abstract
We describe the use of GaAs-based semiconductor optical waveguides for nonlinear frequency conversion of femtosecond pulses in the infrared. Different techniques for the realization of phase matching, including artificial birefringence, quasi-phase-matching and modal dispersion, are reported and analysed and key issues relating to efficiency, practicality and applicability are discussed. Using the data obtained from these experiments, an overall comparison is made with other prominent techniques in order to identify the most promising and viable route to the development of efficient semiconductor waveguide frequency conversion devices for incorporation in the future generation of integrated photonic networks.

Keywords: frequency conversion, semiconductor waveguides, near-infrared, birefringent phase matching, quasi-phase matching, modal phase matching

1. Introduction

The development of novel coherent sources in new regions of the optical spectrum, particularly in the near- and mid-infrared, is of considerable interest for a range of scientific and technological applications. Nonlinear frequency conversion represents an attractive route to the development of such sources due to its simplicity and wavelength flexibility. The potential applications of nonlinear frequency conversion devices in the near- and mid-infrared are diverse, ranging from wavelength and time division multiplexing in telecommunication systems to gas-sensing, time-resolved spectroscopy, material science and bio-photonics [1–12]. Bulk inorganic crystals have been widely established as prime material candidates for nonlinear frequency conversion, but in waveguide format the differential growth currently results in substantial optical losses due to corrugation. Waveguides are preferred to bulk materials due to their capability of maintaining high irradiance throughout the propagation length and compatibility with fibre-based devices. Nonlinear waveguides based on periodically poled oxide ferroelectrics are attractive, but ultimately their use in practical applications may be limited by the stringent alignment tolerances for hybrid coupling between the source and the waveguide. Such a limitation could be eliminated by the use of monolithic integration of the pump source and the nonlinear waveguide, but this technology would not be readily available to this class of devices.

Semiconductor heterostructures offer highly attractive alternative features for the development of novel nonlinear frequency conversion devices. With alterations to the dimensions of the quantum structures and judicial selection of layer composition, the band structure of the microstructures can be engineered to meet particular requirements. The potential also exists for the design of devices exhibiting a specific optical response and operating in a certain frequency

[1] Author to whom any correspondence should be addressed.

range. This symbolizes a distinct advantage over bulk semiconductors, for which the band structure is essentially pre-determined. Among the prospective semiconductor candidates, devices based on GaAs are particularly appealing due to the large second-order nonlinearity [13, 14] of this material ($\chi_{\text{eff}} \sim 100$ pm V^{-1}, which is nearly an order of magnitude higher than that of $LiNbO_3$ [13]), its broad infrared transparency and high optical damage threshold. Other distinct advantages of GaAs nonlinear waveguides over existing materials include room-temperature operation, mature growth and fabrication technology, the possibility of integration with semiconductor laser sources in a monolithic ensemble and the potential for mass production and low cost. On the other hand, a fundamental limitation with GaAs is its optical isotropy, which inhibits birefringent phase matching. To circumvent this problem, a number of techniques have been effectively used to achieve phase matching in GaAs-based waveguide structures, including form birefringence phase matching (BPM) [15–30], quasi-phase-matching (QPM) [31–46] and modal phase matching (MPM) [47–52]. Variations of some of these techniques, demonstrated experimentally and predicted theoretically, include periodic switching of nonlinearity (PSN) in GaAs/AlGaAs waveguide crystals [53, 54], sublattice reversal epitaxy [55], crystal domain inversion [56, 57], orientation patterned GaAs [58–61] and diffusion bonded GaAs crystals [62–65]. There have also been theoretical proposals for phase matching in ordered and disordered $Ga_{0.5}In_{0.5}P$ crystals [66], stacked nonlinear crystals [67] and periodic structures [68]. Here, we present a comparative study of the three main phase-matching techniques of BPM, QPM and MPM based on a comprehensive set of results obtained in experimental second harmonic generation (SHG) of femtosecond pulses in the near-infrared. We also attempt to contrast the relative merits and drawbacks of each technique using the experimental data obtained and compare the demonstrated efficiencies of GaAs-based devices based on these techniques with those resulting from the seminal works in periodically poled lithium niobate (PPLN) waveguides [69–74] and in polymer waveguides [75–84].

2. Birefringent phase matching

Although the first proposal on phase-matched frequency conversion in a laminar structure was in 1975 [15], the experimental realization was not possible until recently due to the difficulty in finding suitable materials possessing sufficiently high nonlinear coefficients and refractive index contrast for form birefringence, essential for this type of phase matching. A highly effective method for the attainment of strong enough birefringence, first demonstrated by Fiore *et al* [16–19], is through selective oxidation of AlAs layers to form Al_2O_3 (Alox) in GaAs/AlAs multi-layered structures. The origin of form birefringence resulting from this process can be understood intuitively by considering the macroscopic crystal formed by the GaAs/Al_2O_3 multilayer system. GaAs is a cubic semiconductor of point group $\bar{4}3m$ and is therefore non-birefringent. The presence of thin Alox layers grown on a (100) substrate breaks the symmetry of three-fold rotation axes and the point group of the new composite material is now $\bar{4}2m$, the same as KDP. This technique was used for the first time

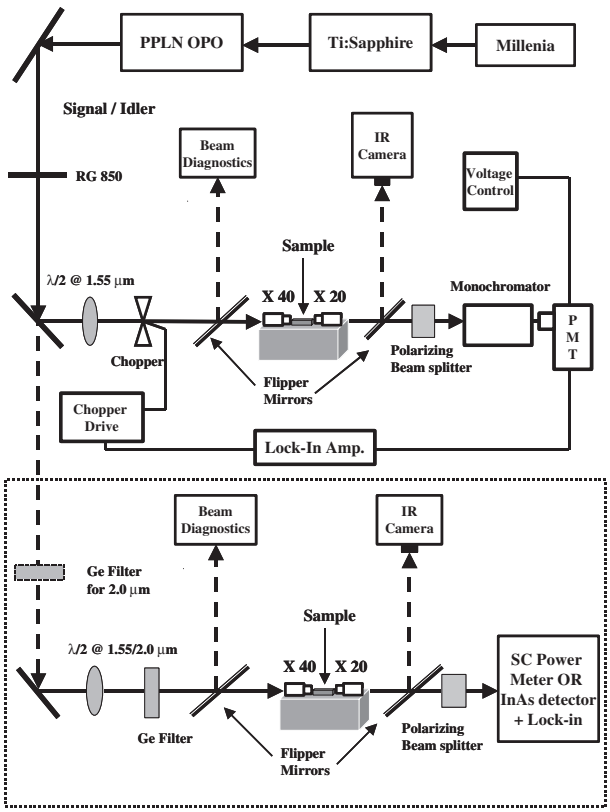

Figure 1. Details of the experimental set-up used for SHG studies.

to demonstrate difference frequency generation (DFG) in the mid-infrared in such structures. Based on form birefringent phase matching, other second-order processes including SHG and parametric fluorescence have also been successfully demonstrated in GaAs-based waveguides [16–29]. Here we describe SHG experiments in birefringent GaAs/Al_2O_3 waveguides using near-infrared femtosecond pulses. The use of femtosecond pulses for frequency conversion is attractive because it offers the potential for the use of GaAs-based waveguides in wavelength- and time-division multiplexing applications for optical telecommunications. Moreover, the high peak intensity of the femtosecond fundamental pulses in our experiments ensures high nonlinear gain and conversion efficiency, while at the same time avoiding optical damage to the waveguides due to low energy fluence resulting from the high pulse repetition rate. SHG studies in GaAs-based waveguides provide useful insights into the design of an integrated optical parametric oscillator (OPO) even though only a part of the broad input spectrum is utilized for nonlinear conversion.

2.1. Experiments

Figure 1 illustrates the experimental set-up employed for our SHG studies. The fundamental source was a synchronously pumped femtosecond OPO based on PPLN. Configuring the OPO in a semi-monolithic cavity design [85] permitted maximum extraction of the idler power, which was used as the source of input fundamental pulses. A Kerr-lens mode-locked Ti:sapphire laser, operating near 820 nm and providing pulses of ∼150 fs duration at 90 MHz repetition rate, pumped

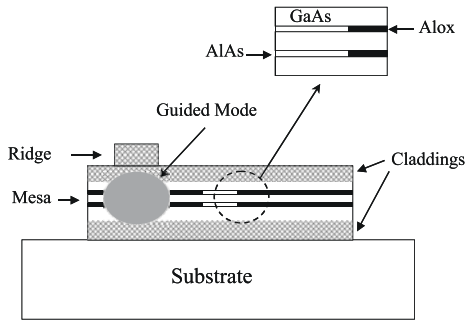

Figure 2. Structure of the GaAs/Alox waveguide used for SHG studies using the BPM technique.

the OPO. The idler pulses from the OPO had durations of ∼200 fs, a spectral FWHM of ∼26 nm and a time–bandwidth product $\Delta\tau\Delta\upsilon \sim 0.36$, indicating nearly transform-limited pulses which were tunable over a range of 1.8–2.1 μm at an average power of ∼50 mW. The beam was chopped with a 50% duty cycle for lock-in detection. An end-fire coupling rig was used for mounting the sample. A half-waveplate placed in the beam path controlled the polarization state of the fundamental pump beam. The TE-polarized fundamental idler pulses from the OPO were focused into the waveguide using a ×40 microscope objective. The transmitted SHG and fundamental were collected using a second microscope objective (×20). This combination of input and output objectives was found to provide the best performance in coupling light into and out of the waveguides. An infrared camera (Micron Viewer 7290A, Electro Physics, sensitive in the 0.4–2.2 μm spectral range) was used for optimizing the coupled fundamental into the waveguide. The average input power was measured using a thermal-head power meter. A germanium filter was placed before the input objective to cut any unwanted residual signal below 1.5 μm. We used a polarizing beamsplitter at the output to separate the TE fundamental and the TM second-harmonic (SH) signals. The transmitted fundamental power was measured using a calibrated InAs detector (sensitive in the 0.5–3.0 μm range) and lock-in amplifier combination. A long-pass quartz filter ($T < 1\%$ for $\lambda \leqslant 1.6\,\mu$m) placed before the InAs detector ensured the exact measurement of only the transmitted fundamental power. The generated SH power was measured using a semiconductor-head power meter.

Figure 2 shows the basic structure of the birefringent waveguides used for the SHG experiments. It consisted of GaAs ⟨001⟩ substrate non-intentionally doped/1000 nm $Al_{0.92}Ga_{0.08}As$/1000 nm $Al_{0.7}Ga_{0.3}As$/4x (50 nm AlAs/250 nm GaAs)/50 nm AlAs/1000 nm $Al_{0.7}Ga_{0.3}As$/30 nm GaAs. Alloy composition and layer thickness were designed for a phase-matched SHG wavelength around 1.0 μm. The waveguide ridges were first etched along the ⟨110⟩ direction in order to exploit the non-zero component of the nonlinear susceptibility tensor $\chi^{(2)}_{xyz}$. Then mesas were also etched permitting the lateral oxidation of all 50 nm thick AlAs layers. The strong refractive index contrast between the semiconductor ($n \sim 3.4$) and Alox ($n \sim 1.6$) results in a form birefringence strong enough to phase match the SHG process. Two samples of different lengths (∼1 and ∼2.2 mm), each with several waveguides of four different widths (4–6 μm), were investigated. Typical linear losses of ∼1 and ∼1.5 cm^{-1} were measured near 2.0 and 1.5 μm, respectively, using a scattering technique [86, 87].

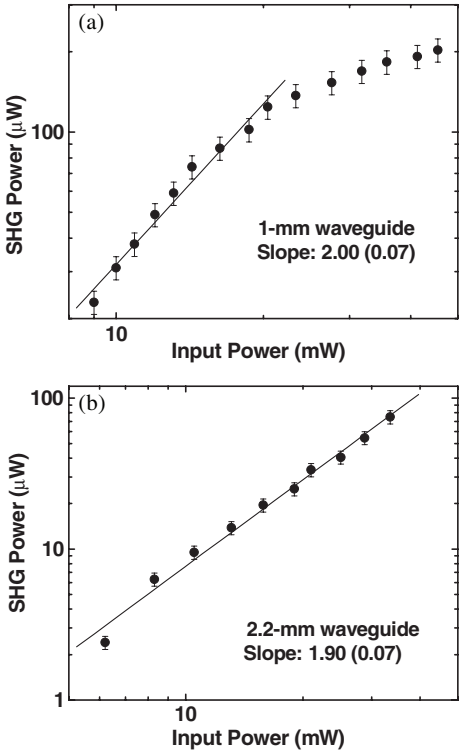

Figure 3. The measured SH power plotted as a function of the fundamental pump power on a log–log plot for (a) a 1 mm sample and (b) a 2.2 mm sample.

2.2. Results and discussion

Figure 3 shows the variation of the generated SH average power with the fundamental power near 2.01 μm. As expected, the SHG power had a quadratic dependence on the input power. The saturation of the generated SH in the shorter sample could be due to different processing conditions leading to different losses for fundamental and SH compared to the longer sample. Figure 4 shows typical spectra of the transmitted pump and SH for a 1 mm long waveguide. The peak of the phase-matching wavelength was centred at a fundamental wavelength of ∼2.01 μm. The input fundamental, shown as the inset to figure 4, had a full width at half-maximum (FWHM) bandwidth of ∼26 nm. The corresponding FWHM spectral width of SH was ∼1.3 nm, indicating that only a part of the total fundamental bandwidth has been utilized in the conversion process. That this is so is clearly verified by the incomplete spectral depletion of the transmitted pump, also shown in the figure. For a 2.2 mm waveguide the FWHM bandwidth of SHG was ∼0.95 nm, as depicted in figure 5. The spectral characteristics shown in figures 4 and 5 were typical of most of the waveguides in the sample. Figure 6 shows typical tuning curves (SH power versus fundamental wavelength) for both 1 and 2.2 mm waveguides. We clearly see a phase-matching peak near 2.01 μm for most of the waveguides, corresponding to $TE_0 \rightarrow TM_0$ interaction. The SHG acceptance bandwidth (FWHM) was ∼35 nm for the 1 mm waveguide, which is somewhat broader than expected (⩽26 nm) due to saturation of the SH, and ∼31 nm for the 2.2 mm waveguide.

To estimate the external efficiency ($P_{\mathrm{SHG}}/P_{\mathrm{FUNDAMENTAL}}$) of the process, we measured the generated SH power directly,

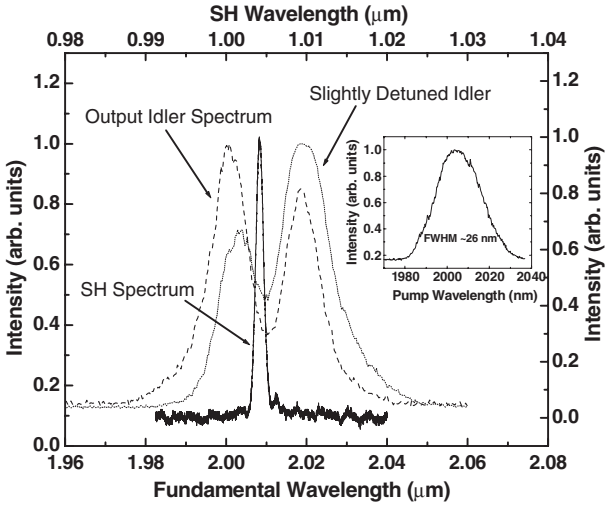

Figure 4. Dotted and broken curves represent respectively the on-resonance and detuned transmitted fundamental spectra with depletion while the full curve represents the corresponding SH spectrum with a FWHM bandwidth ∼1.3 nm for a 1 mm waveguide. The inset shows the fundamental spectrum with a FWHM bandwidth of ∼26 nm.

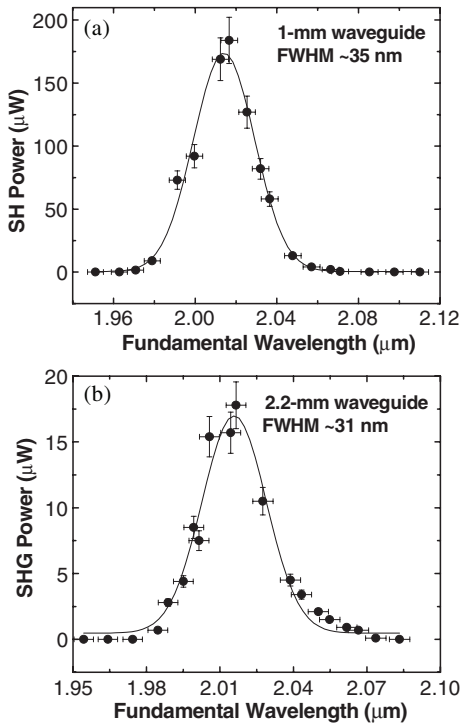

Figure 5. SH power plotted as a function of the fundamental wavelength. The FWHM acceptance bandwidth is ∼35 nm for a 1 mm waveguide and ∼31 nm for a 2.2 mm waveguide.

using the semiconductor-head power meter. For a 2.2 mm waveguide, the maximum usable SH power directly measured on the power meter after the output objective was ∼390 μW for a fundamental power of ∼50 mW measured before the input objective. This represents an overall external efficiency of 0.78%. The maximum power recorded was ∼650 μW for a 1 mm waveguide, corresponding to an overall efficiency of 1.3%. Taking into account the losses from the

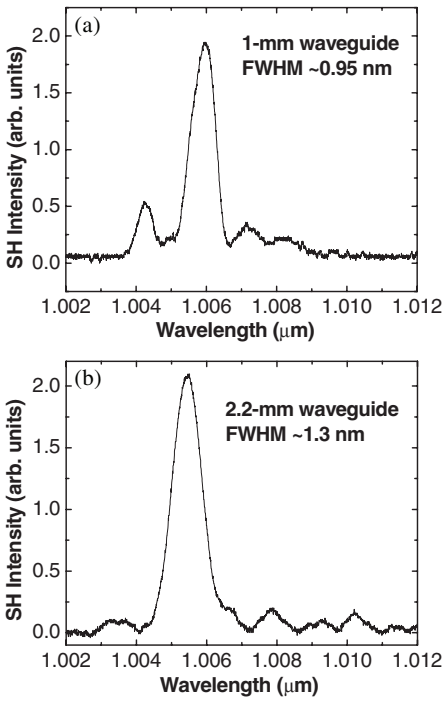

Figure 6. SH spectra obtained for a typical waveguide in (a) a 1 mm sample with a FWHM of ∼0.95 nm and (b) a 2.2 mm sample with a FWHM of ∼1.3 nm.

transmission microscope objectives, waveguide transmission and facet reflectivities, the internal conversion efficiencies are significantly higher. This conclusion is supported by our pump depletion measurements, in which the transmitted pump power was recorded on and off resonance using an InAs detector and lock-in amplifier combination. We observed that, on resonance, typically 30–40% of the pump coupled into the waveguide was depleted (converted into SHG and other loss processes). The validity of pump depletion measurements was also established through the measurements of on- and off-resonance transmitted pump spectra using a highly sensitive monochromator. Although the off-resonance transmitted spectrum was smooth and Gaussian-like, there was a strong dip in the on-resonance spectrum, clearly indicating the depletion of the input fundamental, as can be seen in figure 3(b). Within the conversion bandwidth, the depletion of the fundamental was, in fact, greater than 80%. We also established that any spectral shift within the fundamental bandwidth resulted in no shift in the position of the dip in the transmitted pump spectrum or in the position of the peak in the SH spectrum. These measurements were clear confirmation that the SHG process was indeed phase-matched.

Accounting for the losses from the input microscope objective, waveguide facet reflectivity (∼30%) and geometrical coupling factor (due to the difference in shape of the field outside and modal wavefunction inside the waveguide), we estimate that ∼5 mW of the fundamental power was coupled into the waveguide (for an available input power of 50 mW). Moreover, the detection efficiency at the output of the waveguide was lower than 50%. Considerations of group-velocity mismatch led to an estimate of the effective interaction length shorter than 100 μm. Taking into account the duty cycle

(1.8×10^{-5}), this results in a normalized conversion efficiency [22] of >500% W^{-1} cm^{-2}. Moreover, given that no more than half the fundamental spectrum is utilized in the conversion process, this corresponds to a waveguide conversion efficiency of >1000% W^{-1} cm^{-2}. However, in the presence of femtosecond pulses as used here, the effects of GVD (and possible higher-order nonlinear effects such as self-phase modulation and multi-photon absorption) have also to be considered before an accurate calculation of internal conversion efficiencies can be made. Our loss studies in similar waveguides [86, 87] do indicate strong self-phase modulation effects and the possibility of temporal broadening of the input fundamental, thereby reducing the peak pulse power within the waveguide and overall conversion efficiency. There is further scope to improve the coupling efficiencies, which are very low at present, and thereby increasing the overall efficiency of the device. The use of shorter waveguides and longer input pulses is also expected to lead to higher spectral conversion of the fundamental and possible further improvements in SHG efficiency.

We can compare the conversion efficiency in the present experiments with those obtained from other works based on similar waveguides. Fiore *et al* [19] demonstrated DFG in oxidized GaAs-based waveguides near 4.0 μm with a normalized efficiency of 3% W^{-1} cm^{-2}, which was ~50 times lower than the predicted theoretical efficiency and attributed it to the scattering losses in the mid-infrared. They also reported a SHG efficiency of 0.12% W^{-1} (in our case it was ~10% W^{-1}) in similar BPM waveguides at 1.6 μm with 8 ps input pulses [21]. Bravetti *et al* [22] achieved a much improved DFG efficiency of 500% W^{-1} cm^{-2} near 5.3 μm by optimizing the waveguide design. They predicted that the efficiency could be improved further by minimizing the idler loss of ~50 cm^{-1}. Leo *et al* [23] theoretically predicted a considerable improvement in infrared generation through integration of optical amplification and three-wave mixing. Other second-order nonlinear processes investigated in BPM waveguides include parametric fluorescence studied by Leo *et al* [24] and De Rossi *et al* [26]. These demonstrations enhance the feasibility of developing an integrated OPO using such waveguides. The normalized efficiency obtained in the BPM waveguides described here represents the highest reported to date. The efficiency achieved in the parametric fluorescence experiment (~1000% W^{-1} cm^{-2}) agrees very well with that obtained in our SHG experiment [25]. The high extraction efficiency in our experiments is a result of major improvements in waveguide design and lower propagation losses. Through phase-matching engineering and careful design of layer thickness and sequence in birefringent AlGaAs waveguides, de Sande *et al* [27] theoretically predicted threefold improvement in nonlinear conversion efficiency. Using a number of complimentary techniques, a thorough optical characterization of these waveguides was demonstrated by Leo *et al* [28]. Based on the parametric fluorescence efficiency and the loss measurement results obtained by Rao *et al* [86, 87], De Rossi *et al* [29] have estimated the steady-state cw pump power threshold for an OPO, based on these waveguides, to be ~100 mW. The successful deposition of high quality dielectric mirrors on the end facets of the waveguide would represent a major technological step in the realization of an integrated semiconductor OPO based on such waveguides [30].

A major factor influencing the conversion efficiency in any second-order process is the waveguide propagation loss. We performed loss measurements using two standard methods, namely the cw Fabry–Perot technique and the scattering technique using a tunable femtosecond signal and idler pulses from our OPO [85]. For the birefringent waveguides used in these experiments we obtained linear losses of ~1.0–1.5 cm^{-1} near 1.5 μm and ~1.0 cm^{-1} near 2.0 μm, arising from scattering due to the waveguide and Al_2O_3 (Alox). For wavelengths near 1.5 μm we observed an additional nonlinear loss of ~1.0 cm^{-1}, due to two-photon absorption [86, 87]. We believe that further reductions in the scattering losses and improvements in the overall transmission loss will result in enhancement of the nonlinear conversion efficiency.

3. Quasi-phase-matching

One of the most effective techniques for the attainment of phase matching in a material that lacks inversion symmetry is QPM, achieved through periodic modulation of the nonlinear coefficient [70]. The modulation of nonlinearity could be from a maximum value to zero or can simply be a reversal in the sign of the nonlinear coefficient through domain inversion. In the absence of propagation losses, mth-order QPM, achieved by periodic reversal of the nonlinear coefficient every 'm' coherence lengths, requires 'm' times more coherence lengths to generate the same SH intensity than a first-order QPM. This implies that, for a fixed sample length, the conversion efficiency is $1/m^2$ times lower in mth-order QPM compared to first-order QPM. Earlier reports [31–35] on quasi-phase matched interactions in semiconductors involved the epitaxial growth of $Al_xGa_{1-x}As$ on a patterned substrate, where the periodic crystal domain inversion was achieved using selective etching and wafer bonding. Although this method is direct, efforts were limited by relatively large losses in these structures. An alternative approach is based on the control of the second-order nonlinearities in semiconductor heterostructures by means of quantum well intermixing.

3.1. Sputtered silica defect induced quantum well intermixing

Quantum well intermixing (QWI) represents a range of techniques developed in recent years primarily for the post-growth fabrication of monolithically integrated optoelectronic devices utilizing quantum wells in their active regions [88]. The bandgap shift obtained with these techniques also leads to a modification of the nonlinear optical properties. This can be exploited to achieve QPM in second-order nonlinear processes. The post-growth QPM fabrication techniques using intermixing offer greater flexibility than other alternative phase-matching techniques, including BPM using selective oxidation [20], MPM [47–52] and QPM by domain inversion using growth on patterned substrates [32, 33, 55–58]. Although promising, patterned substrate growth is still associated with high optical losses and low yield. Moreover, in QPM standard growth techniques are used, allowing both the grating period to be subsequently lithographically defined and the possibility of direct integration with active devices such as a pump diode laser or an amplifier. The modulation of $\chi^{(2)}$ in semiconductor waveguides using domain disordered (DD) QPM can be achieved, for example, by implantation, which periodically destroys the lattice symmetry, thus reducing

$\chi^{(2)}$. For the waveguides used in our experiments, DD-QPM was realized through modulation of the heterostructure bandgap, which subsequently provides a modulation in the bulk-like $\chi^{(2)}_{xyz}$ and $\chi^{(2)}_{zxy}$ coefficients when operating near a material resonance. Values for this modulation in GaAs/AlAs superlattices are predicted to be as large as those available in PPLN [42]. A precise means for post-growth control over the bandgap is essential for such a technology, which can be achieved using QWI and thereby lateral control over the heterostructure bandgap can be obtained with no substantial increase in optical losses [37]. In addition, DD-QPM using QWI is attractive since it is based on non-destructive, post-growth, lithography-based semiconductor fabrication. An alternative method for using QWI to obtain DD-QPM is based on the growth of asymmetric heterostructures where additional $\chi^{(2)}$ tensor elements [38] can be induced (xzx, zxx and zzz), which revert to zero upon quantum well intermixing. However, these induced coefficients tend to be relatively small (typically a few pm V^{-1}) [40] and hence the absolute modulation is rather limited.

3.1.1. Experimental procedure. Quasi-phase-matched SHG experiments were initially performed in third-order gratings fabricated using QWI. The structure of the waveguides used comprised 0.6 μm of a symmetric superlattice (SL) waveguide core made of 14:14 monolayers of GaAs:AlAs. The lower and upper cladding was bulk $Al_{0.6}Ga_{0.4}As$ of 1.5 and 1.0 μm width, respectively. A 100 nm GaAs cap was used to cover the upper cladding. The structure was nominally undoped, grown by molecular beam epitaxy (MBE) on a semi-insulating GaAs substrate. The room temperature photoluminescence emission wavelength of the structure was 0.745 μm from the central portion of the wafer. This design allowed the operating fundamental wavelength, ~1.55 μm, at 30 meV below the half-bandgap to avoid two-photon absorption. Domain disordering was achieved using sputtered silica defect induced intermixing [89] with electron-gun-deposited silica caps to suppress the process. After annealing the sample, room temperature photoluminescence peaks were observed at 0.725 and 0.68 μm and the peaks originated from the suppressed and disordered regions, respectively. The fundamental optical source was the femtosecond PPLN OPO described earlier. For these experiments the signal pulses from the OPO were used as the input fundamental. The fundamental pulses, with a duration of ~250 fs and a spectral FWHM bandwidth of ~10 nm ($\Delta\tau\Delta\upsilon \sim 0.33$), were near-transform-limited and tunable over a range of 1.3–1.58 μm at an average power of ~100 mW. The pulses were chopped with a 50% duty cycle for lock-in detection. A 4 mm long sample with third-order grating periods from 5.8 to 12.4 μm was mounted on an end-fire coupling rig. The TE polarized signal from the OPO was launched into the waveguide, while the output from the waveguide was aligned into a monochromator with a 0.1 nm resolution. A photo-multiplier tube (PMT) was used to detect the SH at the output of the monochromator using an internal PMT amplifier and a lock-in amplifier. The response of the PMT was in the spectral range from 185 to 900 nm and therefore no signal resulting from the transmitted fundamental was detected. The power coupled into the waveguide was plotted as a function of the transmitted fundamental power to ensure the linearity of their relation, confirming that there was no significant contribution due to two-photon absorption.

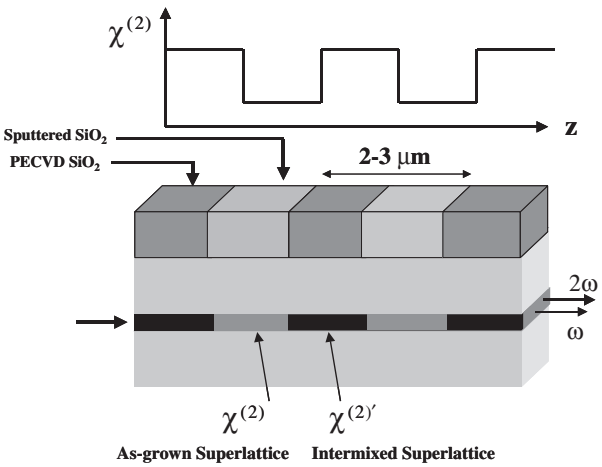

Figure 7. Illustration of a type-I SHG process using QPM. The resonant part of the $\chi^{(2)}_{zxy}$ bulk coefficient is modulated by selective area quantum well intermixing to achieve QPM.

3.1.2. Results and discussion. The periodic modulation in the superlattice bandgap induces a modulation in $\chi^{(2)}$, as illustrated in figure 7, in which intermixing occurs under the sputtered silica caps only. There are two possible phase-matching geometries: (1) type-I phase-matching utilizing the modulation in $\chi^{(2)}_{zxy}$, accessed by launching the input fundamental in TE polarization and the generated SH in TM polarization, and (2) type-II phase matching utilizing the modulation in $\chi^{(2)}_{xyz}$, accessed with a mixed TE + TM polarization for the fundamental and the SH expected in TE polarization. These two cases will be phase-matched at different QPM grating periods due to the variation in the propagation constant with polarization mode. The superlattice breaks the degeneracy between $\chi^{(2)}_{xyz}$ and $\chi^{(2)}_{zxy}$ that exists in bulk semiconductors with a zinc-blende structure, but is restored upon QWI with the larger modulation predicted for $\chi^{(2)}_{xyz}$ [42].

A typical measurement of the SH spectra is shown in figure 8. The SH signal appeared only for TM polarization of the fundamental and there was no signal for TE polarization. The measured FWHM bandwidth of the SH (~3 nm) was limited by finite resolution of the monochromator (minimum slit width) at an acceptable signal-to-noise ratio, whereas the measured FWHM was ~11 nm for the fundamental. Therefore, additional spectral narrowing occurs due to the fact that the bandwidth of the QPM grating was smaller than the input optical pulse duration. The SH signal appeared only when the spectrum of the input fundamental from the OPO was tuned until it contained the appropriate wavelength for the QPM grating under test. Figure 9 shows a typical result for the dependence of the SH power on fundamental power. The best fit to the slope on a log–log plot was ~1.9, confirming the expected quadratic dependence with no saturation observed. SH wavelength as a function of various grating periods available in the sample is plotted in figure 10. As the period of the grating decreased, the QPM wavelength also decreased in this normally dispersive medium.

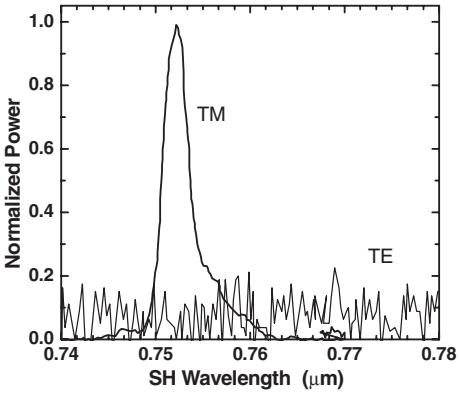

Figure 8. Typical SH spectra showing both output polarizations. The waveguide had a QPM grating period of 12.4 μm.

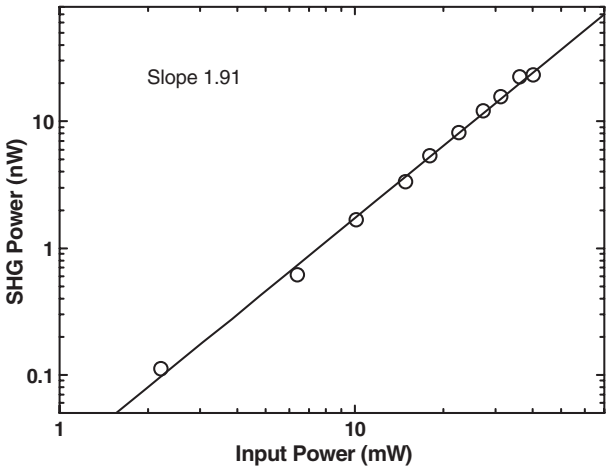

Figure 9. The SH output average power (measured at the PMT) as a function of the fundamental input average power (measured after the chopper) on a log–log scale. The best fit to the slope is 1.9.

The largest average SH power measured was ∼25 nW near 0.758 μm. However, the optical measurement system had a transmission loss of ∼5 dB between the waveguide and PMT, and with a further 30% reflection loss at the rear facet of the waveguide, we determined the best average SH power to be ∼110 nW in the waveguide. In this case, we measured a transmitted fundamental average power of 250 μW which, with a 30% loss at the rear facet and a measured optical loss of ∼2 dB cm^{-1} in the waveguide, translates to an average pump power of ∼450 μW just after the front facet of the waveguide. We observed a reduction of approximately two orders of magnitude in the fundamental power between the OPO output and the guided mode, which is principally due to coupling losses. Hence, we obtain a maximum SH conversion of ∼0.02%, for which there is considerable scope for improvement:

(1) The coupling losses severely limited the fundamental power launched into a guided mode.
(2) The bandwidth of the fundamental was larger than the QPM grating and hence the majority of the guided fundamental was not phase-matched. Furthermore, dispersion will result in significant temporal broadening of the fundamental pulse leading to variation in the peak irradiance along the propagation length.

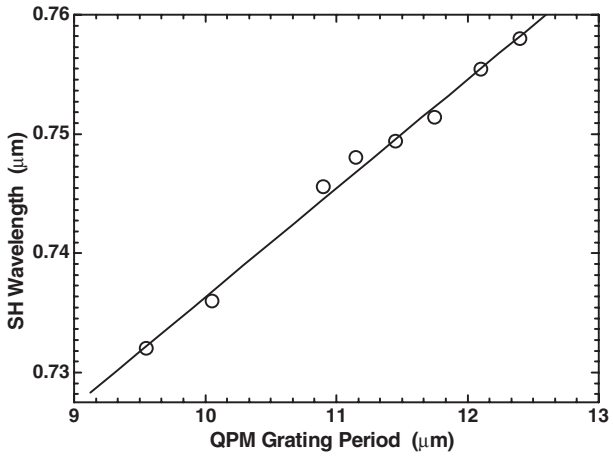

Figure 10. SH wavelength plotted as a function of QPM grating period in the waveguides.

(3) In the present waveguide a third-order grating was used in order to ensure the resolution of the intermixing process is sufficient.

However, the period of the grating for phase matching was larger than our first estimates and first-order gratings should be feasible with potentially an order-of-magnitude improvement in conversion efficiency. While not characterized thoroughly, we did observe SHG by first-order QPM using our shortest grating period at the long-wavelength limit of the fundamental pulses.

3.2. Ion-implantation-induced QWI

One of the major disadvantages of DD-QWI is that the sample processing required for the necessary micron-scale resolution is difficult to reproduce and conversion efficiency improvements have proved elusive in spite of extensive process development and optimization [45]. These fabrication limitations may be unavoidable as the sputtered silica process creates group III vacancies at the wafer surface, which then have to migrate across the waveguide cladding and the core regions to promote intermixing and some lateral spreading is inevitable. Previous reports indicate the necessity to obtain the spatial resolution required for first-order gratings, even if higher-order gratings are used [45]. Bouchard *et al* [44] used ion-implantation-induced intermixing [91] in an asymmetric AlGaAs quantum well waveguide based on modulation in the induced, but far smaller, $\chi^{(2)}_{zzz}$ coefficient. We later concentrated our efforts on first-order quasi-phase-matched SHG based on ion-implantation-induced intermixing using the larger modulation obtained with the bulk-like $\chi^{(2)}_{zxy}$ coefficient. We observed considerable improvement in the conversion efficiency, enabling us to simply use a power meter for the detection of the generated SH signal.

3.2.1. Experiments. For a fundamental wavelength at 1.5 μm, the period of the first-order grating was calculated to be ∼3.7 μm using the effective refractive index data measured using a coupler grating technique [92]. A rib waveguide structure was used in order to maintain overlap of the fundamental and SH intensities over a sufficient interaction

air	
GaAs	100 nm
$Al_{0.60}Ga_{0.40}As$	800 nm
$Al_{0.56}Ga_{0.44}As$	300 nm
150 layer superlattice	600 nm total
75 layers AlAs	4.0 nm each
75 layers GaAs	4.0 nm each
$Al_{0.56}Ga_{0.44}As$	300 nm
$Al_{0.60}Ga_{0.40}As$	4000 nm

Figure 11. Structure of a superlattice waveguide wafer used in QPM SHG studies using ion-implantation-induced QWI.

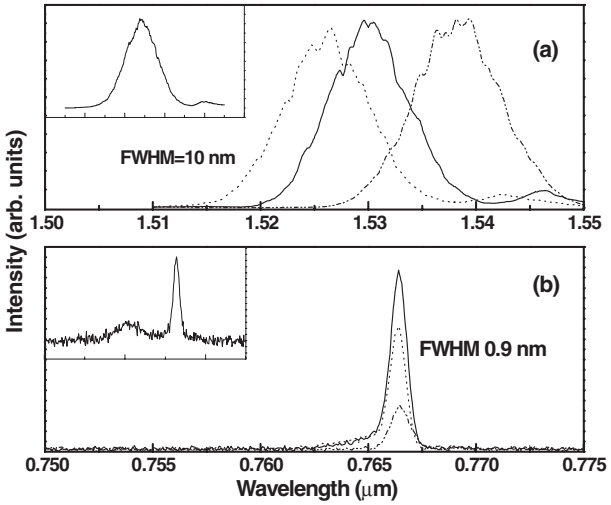

Figure 12. Observed SH (b) and the fundamental (a) spectra. The inset shows the corresponding spectra on an expanded vertical scale at a detuning of ∼10 nm, where both phase-matched and non-phase-matched components are evident.

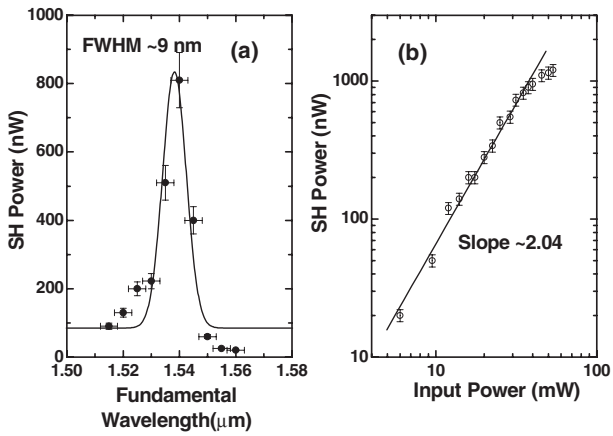

Figure 13. (a) Measured wavelength-tuning curve for SHG with FWHM acceptance bandwidth of ∼9 nm. (b) The SH average power as a function of fundamental input average power on a log–log scale. The best fit (full line) to the slope is 2.04.

length for the nonlinear process to proceed efficiently. The layer structure of the sample used in the present study is shown in figure 11. A loss measurement at a wavelength of 1.55 μm, based on a Fabry–Perot technique, yielded a value of $\sim$4.8 cm^{-1} in the QPM sample implanted with an ion dosage of 10^{14} ion cm^{-2}, which was employed for the nonlinear measurements. Complete details of sample fabrication can be found elsewhere [46].

A 2 mm long sample with first-order grating period was mounted on the end-fire coupling rig described previously. Linearly polarized light from the OPO was launched into the waveguide, with the output of the waveguide aligned onto a semiconductor power meter. A typical measurement of the SH spectra, obtained using an optical spectrum analyser, is shown in figure 12. As expected for type-I phase matching, the detected SH signal was TM-polarized with a TE fundamental polarization, with no SH signal for the TM-polarized fundamental. The measured bandwidth of the fundamental was ∼10 nm (FWHM) while that of the SHG, determined by the finite bandwidth of the QPM grating, was ∼0.9 nm. The SHG signal appeared only when the output spectrum of the OPO was tuned to provide the appropriate wavelength for the QPM grating under test. By tuning the pump away from the phase-matching wavelength, we also observed a broad-bandwidth non-phase-matched output signal at lower power levels. This is depicted in the inset of figure 12, where the fundamental was detuned by ∼10 nm with respect to the optimal phase-matching wavelength.

3.2.2. Results and discussion. The measured average SH power is plotted as a function of peak fundamental wavelength in figure 13(a). As the source is not monochromatic, the lineshape is determined by the fundamental spectrum rather than the usual $\sin c^2$ function. Figure 13(b) shows a typical result for the dependence of the average SH power on the fundamental power. The best fit to the slope on a log–log plot was 2.04, confirming the expected quadratic power dependence. A saturation of the SH power started for input powers above 40 mW. With a decrease in grating period the phase-matched SH signal shifted to shorter wavelengths, as expected with normal dispersion. The lower wavelength limit is reached when the SH photon energy approaches the material bandgap and experiences excessive band-edge absorption. Using longer grating periods, we were also able to observe third-order QPM with an appropriate drop in the generated SH power levels. The use of a femtosecond source introduces several unknown factors (see below) in the determination of conventional conversion efficiencies. However, we are able to make comparisons with previous experiments by noting that the largest average SH power measured was ∼1.5 μW at a wavelength of 0.767 μm. Taking into account the estimated 5 dB loss between waveguide and detector and 30% reflection loss at the rear facet of the waveguide, we estimate an average SH power of ∼7 μW generated within the waveguide. The average power in the transmitted fundamental was ∼2.9 mW which, with a 30% loss at the rear facet and a measured optical loss of ∼4.8 cm^{-1} in the waveguide, translates into an average fundamental power of ∼11 mW just after the front facet of the waveguide. This corresponds to an end-fire coupling efficiency of around 18%. Therefore, we obtain a maximum SHG conversion of ∼0.06% with the present set-up, for which

there is considerable scope for improvement:

(1) Partial utilization of the total available bandwidth of the fundamental.
(2) Dispersion will result in significant temporal broadening of the fundamental pulses, thereby reducing the peak irradiance as it propagates in the waveguide. A transform-limited picosecond optical source would avoid both of these restrictions.
(3) The nominal 50:50 square-wave QPM grating duty cycle is likely to be considerably modified by the defect out-diffusion at high annealing temperature in addition to the ion implantation lateral straggle.
(4) The optical losses are slightly high in comparison to previous intermixed waveguides. This may be partly due to the surface damage caused by the gold etch and an additional protective silica layer is being introduced in future samples to avoid this. It may also be desirable to use a lower ion dosage to trade-off some of the modulation of the nonlinear coefficient for lower losses.
(5) Furthermore, it has been predicted that the associated modulation in the linear refractive index ($\Delta n \sim 0.01$ has been measured at $\lambda \sim 1.55$ μm for this wafer structure intermixed using the sputtered silica cap process [90]) will also compromise conversion efficiency by around 30% [93, 94].

Comparing the efficiencies obtained in our QPM waveguides with other works based on similar technique(s), Yoo *et al* [32] observed QPM SHG at 1.466 μm in AlGaAs waveguides, epitaxially grown on a template substrate where a periodic domain inversion was achieved using wafer bonding and organometallic chemical vapour deposition, with a conversion efficiency of 4.9% W^{-1}. This was about 25 times lower than the theoretical prediction and is attributed to large scattering losses, unequal domain boundary dimensions and grain boundary effects. Yoo *et al* [33] again achieved a much-improved efficiency of 15% W^{-1} at 1.54 μm in AlGaAs waveguides due to a tighter optical confinement realized by a buried heterowaveguide. Janz *et al* [34] reported surface-emitted SHG near 1.55 μm from a QPM waveguide in $Al_xGa_{1-x}As/Al_2O_3$ microcavity with an efficiency of 5×10^{-3}% W^{-1}. Bouchard *et al* [41] measured an effective nonlinear susceptibility modulation of 0.02 pm V^{-1} in the 1.5–1.6 μm spectral range in $Al_xGa_{1-x}As$ asymmetric quantum-well waveguides using SHG experiments, where the QPM was realized using ion-implantation-induced intermixing. SHG in domain inverted AlGaAs near 1.51 μm was reported by Xu *et al* [53] with an output power of ~0.2 nW for an input power of ~475 μW and a conversion efficiency of ~1.4%. Xu *et al* [54] again using AlGaAs QPM waveguides having periodically domain-inverted structure reported sum frequency generation (SFG) (1.54 + 1.575 μm) with a normalized conversion efficiency of 810% W cm^{-2} for a 0.5 mm sample. However, the optical loss in their sample was ~23 cm^{-1}. They could extract ~0.3 nW of SFG power for 0.0165 mW^2 of pump power. Evaluating the above results, we extracted a conversion efficiency of ~5.8% W^{-1} in the ion-implantation intermixed waveguides corresponding to a device conversion efficiency of ~0.06%, which could be considerably improved as discussed in the previous section. More significantly, we achieved practical SH power levels of a few microwatts.

4. Modal phase matching

Modal phase matching (MPM) is a simple solution to the problem of phase velocity synchronism in nonlinear frequency conversion processes and is well known [47, 48], but has been of limited interest because of the poor spatial overlap between the interacting modes. Waveguides generally support several modes, each with different propagation constants (effective refractive indexes, n_{eff}). This index is lower for higher-order modes and therefore phase matching in SHG ($n_{\text{eff}}^{\omega} = n_{\text{eff}}^{2\omega}$) can occur if the fundamental mode propagates in a lower-order mode than the SH. Also, by use of proper waveguide design, the overlap integral between the third-order mode and the fundamental can be optimized, resulting in a still appreciable effective nonlinearity. Very recently, Chowdhury *et al* [49] and Oster *et al* [50, 51] theoretically proposed new M-type waveguide structures in $LiNbO_3$ and GaAs, respectively, with enhancement in modal overlap. One of the early demonstrations of MPM in GaAs optical waveguides was by Anderson *et al* [47] near 10 μm and van der Ziel *et al* [48] at 2 μm. There have been several other theoretical and experimental realizations of MPM in a variety of polymer and ZnTe waveguides [95–100]. The expected normalized conversion efficiency, $P_{\text{SH}}/(P_{\text{FF}}^2 L^2)$, in optimized structures is a factor of 20 lower than in birefringent semiconductor waveguides and it is comparable with PPLN. On the other hand, there is no need for selective oxidation (as in the case of BPM waveguides) and so the structure can be combined with a laser diode on the same chip to provide a wholly integrated semiconductor source of tunable light based on nonlinear frequency conversion. Such a device could be of interest for a range of applications, for example as a source of entangled photons in quantum optics and quantum cryptography [101, 102].

4.1. Experiments

The sample was grown on a semi-insulating GaAs substrate by a Varian MBE machine. The epitaxial structure used was 1000 nm $Al_{0.98}Ga_{0.02}As$/130 nm $Al_{0.25}Ga_{0.75}As$/260 nm $Al_{0.50}Ga_{0.50}As$/130 nm $Al_{0.25}Ga_{0.75}As$/1000 nm $Al_{0.98}Ga_{0.02}As$/30 nm GaAs. Optical ridges were etched chemically in order to provide 2D confinement. Ridge width varied from 3 to 5 μm and the waveguide length was initially 3.0 mm. The optimized structure is a type of 'M' waveguide, designed for maximum overlap between the TE_2 (third-order) mode at the SH wavelength and the TE_0 and TM_0 modes at the fundamental wavelength (figure 14(a)). We utilized a type-II phase matching scheme, allowed by the selection rules of GaAs second-order susceptibility tensor in the case of a $\langle 1, 0, 0 \rangle$ growth, and a waveguide oriented along the $\langle 0, 1, 1 \rangle$ axis [47]. Type-I phase matching is also possible (TM_2 at SH and TM_0 at fundamental) at slightly shorter wavelengths. Overlap is enhanced by the characteristic 'M' profile of the waveguide core as shown in figure 14(b). A comprehensive theoretical study of this structure is reported in [49] and [50]. The losses at 1.55 μm, measured using the scattering technique, were ~2.7 cm^{-1} for TE input polarization and ~3.5 cm^{-1} for TE + TM input polarization. Near 0.82 μm, the losses were ~1.1 cm^{-1} for TE polarization and ~1.0 cm^{-1} for TM

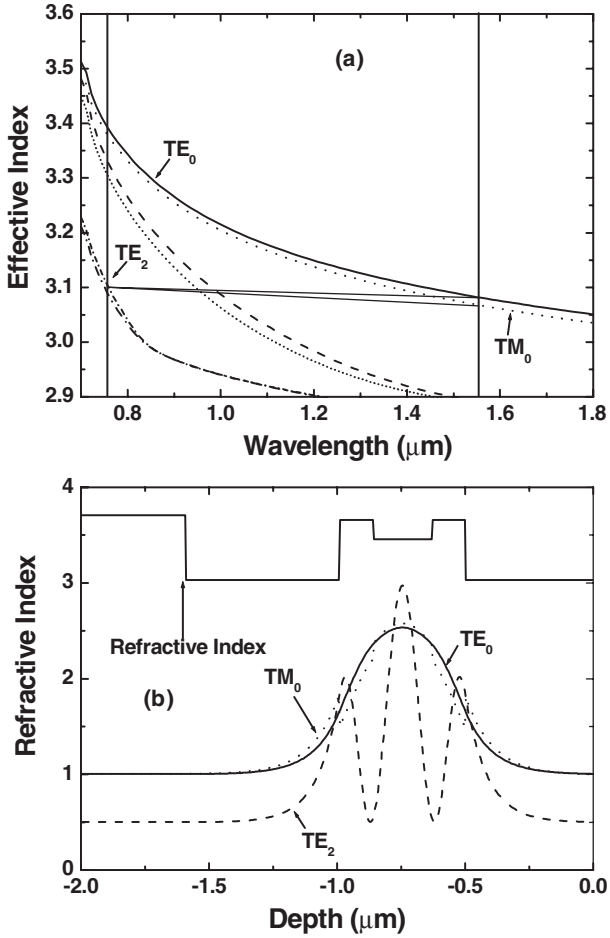

Figure 14. (a) Dispersion of the effective indexes of the first three modes in both polarizations (TE (full) and TM (broken) curves), illustrating the principle of modal phase matching: chromatic dispersion is compensated with the waveguide dispersion. The waveguide geometry is defined such that the third-order mode at 0.775 μm has the same phase velocity as the fundamental mode at 1550 nm. (b) Waveguide refractive index and intensity distribution $|E^2|$ of modes TE_0 and TM_0 at 1.55 μm and TE_2 at 0.775 μm.

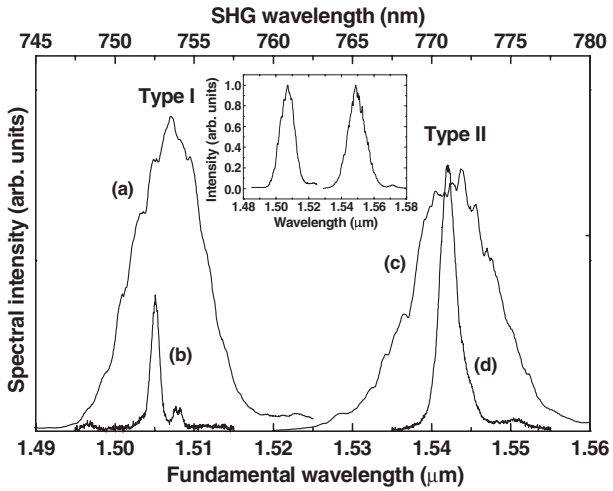

Figure 15. Typical transmitted fundamental spectra (curves (a) and (c)) for type-I and type-II interactions, respectively, and the corresponding SHG spectra (curves (b) and (d)). Input spectra are provided in the inset. The vertical axis indicates the relative strength of each process.

polarization. However, it is very difficult to estimate the losses at the SH using either the scattering or Fabry–Perot techniques as this requires a second-order mode. The experimental set-up was similar to the one described in earlier sections. Near-transform-limited fundamental pulses of ∼250 fs duration and ∼10 nm spectral FWHM with average power levels of ∼70 mW were used. A long-pass filter blocked any residual light below 0.85 μm, while a half-waveplate controlled the input fundamental polarization. A semiconductor head power meter, sensitive only in the spectral range from 0.4 to 1 μm, was used to measure the SHG power.

4.2. Results and discussion

A clear growth of the SHG signal was observed for appropriate tuning of the fundamental wavelength and for both TE and TE + TM input polarizations. A polarizing beamsplitter inserted before the power meter allowed the investigation of the polarization state of the generated signal. It was established that the generated output was TM (TE) polarized for TE (TE + TM) input, indicating phase-matched type-I and type-II interactions, respectively. An infrared spectrum analyser was used to record the spectra of the generated SH as well as the transmitted fundamental. A typical set of spectra, supporting phase-matched SHG, is shown in figure 15. It is evident that a type-I process takes place at ∼1.505 μm and a type-II at ∼1.540 μm. The corresponding SHG spectra present a FWHM spectral width of ∼0.5 and ∼1 nm, respectively. These values are consistent with the estimate of the spatio-temporal evolution model. In the present case, the fundamental had a spectral FWHM of ∼10 nm (shown as an inset of figure 15). Therefore only a fraction of the input bandwidth is used in the conversion process. This effect can be viewed in the temporal domain as only a part of the pump wavepacket having a phase velocity that can be matched at the SH. When the conversion efficiency is high enough, the pump experiences a partial depletion reminiscent of spectral hole burning. This has indeed been observed in form birefringent waveguides [25]. Under the same experimental conditions, no depletion of the fundamental was observed using modal phase-matched samples, thus indicating lower conversion efficiency. Further evidence of phase matching was obtained by measuring the generated SH power as a function of the fundamental power. The expected quadratic dependence was confirmed, with typical values of the best fit to the slope on a log–log plot ranging from 1.9 to 2.1. Figure 16 shows a representative set of such measurements for the same waveguide and for both type-I and II interactions. A small reduction in the slope could be observed for a number of waveguides for input average power levels above ∼30 mW. We also observed non-phase-matched SHG, which was ∼25 times lower in magnitude than the phase-matched signal, with a FWHM of ∼5 nm, providing strong evidence that we were characterizing a phase-matched process. The generated SH power was also measured against the central wavelength of the fundamental spectrum for fixed input power, as shown in figure 17. A clear peak was observed at ∼1.505 μm (∼1.540 μm) for type-I (II) interaction. The spectral acceptance (bandwidth of the SH

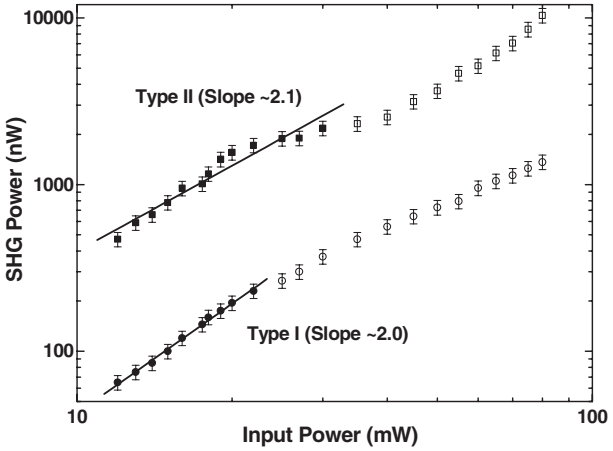

Figure 16. The second-harmonic average output power as a function of the fundamental average power. Scattered points are the experimental data and the full lines are the best fits.

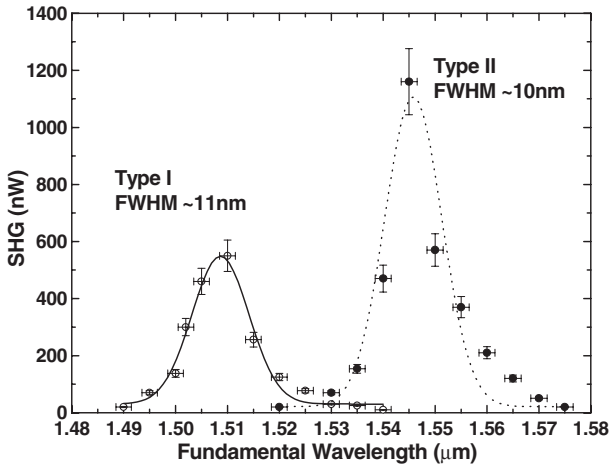

Figure 17. phase-matching acceptance bandwidth curve showing the SHG power as a function of the fundamental centre wavelength. Scattered points are the experimental data and the full curves are the best fits.

signal versus pump central wavelength curve) depends on the convolution of the pump spectra with the true phase-matching spectral acceptance. A FWHM acceptance bandwidth of ∼11 nm (∼10 nm) was calculated for the type-I (II) process.

Maximum SHG power was measured after cleaving the sample to 1.5 mm. For type-I interaction we measured up to 2.6 μW of SH power after the output objective for 80 mW of input power before the input microscope objective. For type-II interaction we detected up to 10.3 μW of SH power for 65 mW input. These values represent an increase of more than 50% compared to the initial 3 mm long waveguides, indicating high SH transmission loss. It should be noted that, while using ∼250 fs pulses, the interaction length, limited by group velocity mismatch (GVM), is shorter than the waveguide length. Therefore, a longer device tends to have a lower yield owing to propagation losses at the SH. The maximum external efficiency (SH power collected after the output objective divided by the launched fundamental power before the input objective) of the present device was ∼0.015% for type-II geometry. A qualitative comparison of BPM and QPM SHG in III–IV waveguides using the same set-up shows that the efficiency of the present scheme is of the same order of magnitude as the one obtained by the QPM device reported by Zeaiter *et al* [46]. However, it is almost two orders of magnitude lower than the efficiency obtained in form birefringent waveguides reported by Moutzouris *et al* [25], where ∼650 μW of SH power was obtained. To explain such low values in the present waveguides, we need to consider a number of factors. We estimated that less than 20 mW of fundamental power is actually coupled into the waveguide, accounting for the losses due to the input objective, the input facet reflectivity and the mode-matching factor. This is well supported by our measurements, which showed that only ∼7% of the available input power is actually collected after the output objective. This factor is about the same order as in [25]. The collection efficiency of the generated SH was less than 30% (lower than in [25]), because of high divergence and high reflectivity (the modal reflectivity could be as high as ∼50% according to the model of [103]). Based on the above factors, an internal efficiency (coupled fundamental power divided by the generated SH power in the waveguide) of >0.15% was estimated for type-II interactions. An estimated interaction length of ∼100 μm indicates that the actual conversion efficiency could be even higher. The main difference between birefringent waveguides operating on fundamental modes and MPM waveguides is the overlap integral (∼0.6 $\mu m^{-0.5}$ in the case of BPM and ∼0.14 $\mu m^{-0.5}$ in the case of MPM), yielding a factor of 20 in difference. The additional factor of 5 could be explained with a rather poor confinement of the SH wave.

5. Efficiencies achieved using various techniques

Although all the above-mentioned techniques are quite different, we performed these studies under similar experimental conditions including the same optical source, same focusing optics and detection systems. Therefore, we may reasonably compare the results of these experiments on a qualitative, if not quantitative, basis. The BPM samples provided the maximum output power among the several samples we investigated using different techniques. Without even considering the exact details of the coupling factors, losses and normalized efficiencies, the maximum output powers obtained in BPM, QPM and MPM experiments were ∼650, ∼2 and ∼10 μW, respectively, for input powers of ∼60 mW, clearly indicating that these are practically usable powers in many applications. By employing even better waveguide design, improved coupling efficiency, lower fundamental and nonlinear wavelength losses, these waveguides could be pushed into the mW output power regime. Table 1 shows the results of frequency conversion experiments, performed by various groups over the last decade, in semiconductor, PPLN and polymer waveguides. Rafailov *et al* [50, 51] demonstrated SHG from a first-order QPM GaAs/AlGaAs waveguide crystal using periodic modulation of the nonlinear coefficient and predicted a conversion efficiency of 0.1% near 2.0 μm. Koh *et al* [52] devised sublattice reverse epitaxy of GaAs/Ge/GaAs and achieved a normalized internal conversion efficiency of 2.0×10^{-3}% W^{-1} near 1.575 μm, which was three orders of magnitude lower than the predicted theoretical efficiency of 1.5% W^{-1}. The low efficiency was attributed to high waveguide losses that were in-

Table 1. Comparison of the efficiencies obtained for various samples and different techniques.

Sample	Technique	Input power/energy	Output power	Efficiency	Norm. efficiency (% W^{-1} cm^{-2})	Source(s)	Reference
AlGaAs/AlAs	BPM/DFG	0.44 mW^2	90 pW	—	3.0	cw, 1.32 + 1.0 μm	[19]
GaAs/Alox I	BPM/SHG	1.1 mW	2.3 μW	0.21%	4.5	8 ps, 1.605 μm	[21]
GaAs/AlAs	BPM/DFG	7 mW^2	0.12 μW	—	500	cw, 1.32 + 1.0 μm	[22]
GaAs/Alox II	BPM/SHG	50 mW^a	650 μW	1.3%	>1000	200 fs, 2.01 μm	[25]
AlGaAs	BPM/Par. Fl.	—	4 nW	—	1000	cw, 0.95–1.064 μm	[26]
GaAs/AlAs I	QPM/SHG	2.3 mW^d	25 nW	0.02%	—	250 fs, 1.48–1.52 μm	[43]
GaAs/AlAs II	QPM/SHG	9.0 mW^d	1.5 μW	0.06%	—	250 fs,1.534 μm	[46]
AlGaAs	QPM/SFG	0.0165 mW^2	0.4 nW	—	810	cw, 1.54 + 1.575 μm	[57]
AlGaAs	QPM/SHG	—	—	4.9% W^{-1}	—	cw, 1.466 μm	[32]
AlGaAs	QPM/SHG	—	—	15% W^{-1}	—	cw, 1.542 μm	[33]
$Al_xGa_{1-x}As$	QPM/SHG	—	—	—	0.02 pm V^{-1} [b]	cw,1.48–1.62 μm	[44]
MgO:$LiNbO_3$	QPM/SHG	12.3 mW	1.2 mW	—	1000	cw, 0.75–0.84 μm,	[108]
PPLN	QPM/SHG	—	—	—	150	cw, 1.5365 μm	[74]
Ti:$LiNbO_3$	QPM/DFG	2 mW + 110 μW	—	105% W^{-1}	1.6	cw, 1.56 + 3.39 μm	[104]
MgO:$LiNbO_3$	QPM/SHG	42 mW	5.5 mW	—	1200	cw, 0.867 μm	[105]
$LiTaO_3$	QPM/SHG	34 mW	4.5 mW	13%	—	Quasi-cw, 0.856 μm	[107]
Polymer	QPM/SHG	—	—	—	0.05	6 ps, 1.62 μm	[82]
GaAs/AlAs	MPM/SHG	65 mW	10.3 μW	0.15%	—	250 fs, 1.505/1.54 μm	[52]
Polymer	MPM/SHG	133 mW	1.2 μW	—	39	cw, 0.815 μm	[95]
Polymer	MPM/SHG	—	—	—	14	6–8 ps, 1.55 μm	[79]
Polymer	MPM/SHG	4.5 mW	38 μW	—	245	95 fs, ~0.8 μm	[83]
GaAs/Ge/GaAs	OPQPM/SHG	—	—	0.002% W^{-1}	—	cw, 1.5761 μm	[55]
GaAs/AlGaAs	PSNQPM/SHG	1 mW	1 μW	0.1%	—	250 fs, 2.0 μm	[54]
AlGaAs	CDI[c]/SHG	475 μW	0.2 nW	1.4% W^{-1}	—	cw, 1.5118 μm	[56]
GaAs	OPQPM/SHG	100 μJ	—	33%	—	65 ns, 4.135 μm	[58]
AlGaAs	OPQPM/SHG	10 mW	2 nW	—	—	1.564 μm	[59]
GaAs	Diffusion Bonding/SHG	—	—	24%	—	60 ns, 10.59 μm	[63]
GaAs	Diffusion Bonding/DFG	17 mJ	2 μJ	0.034%	—	60 ns, 1.95 + 2.34 μm	[64]

[a] Coupled power ~5 mW. [b] Effective nonlinear susceptibility modulation. [c] Crystal domain inversion. [d] Estimated power near the front facet.

duced by corrugation of the guide layer. Using all-epitaxially-fabricated thick, orientation-patterned GaAs films, Eyres *et al* [58] demonstrated SHG with a fundamental near 10.0 μm and obtained efficiencies close to 4×10^{-3}% W^{-1}. Skauli *et al* [55] designed quasi-phase-matched orientation-patterned GaAs structures by a combination of molecular-beam epitaxy and hydride vapour phase epitaxy and obtained an internal conversion efficiency of 33% in their SHG experiment using an uncoated sample with nanosecond pulses near 4.0 μm. Yu *et al* [56] fabricated low-loss orientation-patterned AlGaAs waveguides and obtained 2 nW of SHG power, for an input power of 10 mW at 1.56 μm, comparable to an estimated output power of 20 nW. The transfer of corrugation of the template to the waveguide core resulted in high transmission losses for both fundamental and SHG. Lallier *et al* [60] achieved efficient SHG (~24%) of a 10.6 μm, 60 ns CO_2 laser pulse with a quasi-phase-matched diffusion bonded GaAs crystal. Lallier *et al* [61] also reported an infrared DFG conversion efficiency of 3.4×10^{-4} with diffusion-bonded QPM GaAs at 11.35 μm using a $LiNbO_3$ OPO. For an input energy of 17 mJ they detected 2 μJ of DFG energy (~180 W of peak power).

Among the various reports of frequency conversion in other waveguides [104–111], only $LiNbO_3$ and doped $LiNbO_3$ waveguides have proved marginally more efficient (in terms of recorded output power and internal efficiency) than the reported structures in the present study, with a few of the $LiNbO_3$ experiments in the visible range. One of the first reports of mid-infrared generation in PPLN waveguides was by Lim *et al* [69], who reported 1.8 μW of 2.1 μm radiation for 160 mW of 0.81 μm and 1 mW of 1.32 μm radiation coupled into the waveguide, corresponding to a normalized efficiency of ~4% W^{-1} cm^{-2}. Very recently, Parameswaran *et al* [74] achieved the highest normalized SHG conversion efficiency of 150% W^{-1} cm^{-2} in the 1.5 μm communication band in buried waveguides formed by annealed and reverse proton exchange in PPLN. Hofmann *et al* [104] produced mid-infrared radiation near 2.8 μm though QPM DFG in periodically poled Ti:$LiNbO_3$ channel waveguides by mixing 1.55 μm radiation from a diode laser and 3.391 μm radiation from a He–Ne laser. They obtained a conversion efficiency of 105% W^{-1} corresponding to a normalized value of 1.6% W^{-1} cm^{-2}. Mizuuchi *et al* [105] achieved a normalized SHG conversion efficiency of 1200% W^{-1} cm^{-2} in x-cut MgO:$LiNbO_3$ waveguides using QPM and Nb_2O_5 as a cladding layer. They observed 5.5 mW of SHG power for a pump power of 42 mW at a fundamental wavelength of 0.867 μm. Sugita *et al* [108a] successfully generated highly efficient (1000% W^{-1}) ultraviolet light at 0.386 μm in periodically poled MgO:$LiNbO_3$ waveguides. Sato *et al* [109] demonstrated a QPM-DFG device for the 1.5 μm band using annealed-proton-exchanged PPLN waveguides with a high-index cladding layer of As_2S_3, which enhanced the mode overlap, thereby improving the efficiency. They observed a normalized SHG conversion efficiency of 790% W^{-1} for a

fundamental wavelength of 1.533 μm. They also estimated a DFG conversion efficiency of -6 dB at 1.528 μm for 30 mW of pump power (1.534 + 0.765 μm).

Amongst an array of polymer waveguides investigated for frequency conversion using QPM and MPM techniques, Jäger *et al* [79] demonstrated an efficient SHG of 14% W^{-1} cm^{-2} in overdamped polymeric channel waveguides using modal dispersion phase-matching near 1.55 μm using 6–8 ps pulses from a colour centre laser. Wigres *et al* [81] obtained efficiencies up to 7% W^{-1} cm^{-2} with an optimized overlap integral for modal dispersion phase-matched SHG in a new class of polymer waveguides. Jäger *et al* [82] also reported SHG in poled polymer channel waveguides at 1.5 μm utilizing the QPM technique. Using 6–9 ps pulses they achieved an efficiency of 0.05% W^{-1} cm^{-2}. They suggest that, in order to utilize the high nonlinearity of polymers, better geometry, poling procedure and materials are critical to realize complete modulation of the nonlinearity. The highest efficiency (up to 245% W^{-1} cm^{-2}) in a polymer waveguide was achieved by Dai *et al* [83a] for an interaction length of 36.7 μm working with high repetition rate 100 fs pulses from a Ti:sapphire laser. Very recently, Martin *et al* [83b] reported quasi-phase-matched second harmonic generation in a polymer channel waveguide consisting of disperse red one (DR1) grafted to a poly(methylmethacrylate) (PMMA) main chain polymer at 30% molecular weight concentration with an experimental efficiency of 0.023% W^{-1} at 1.536 μm.

It is clearly evident from the above discussion and the values presented in table 1 that the semiconductor waveguides have excellent performance compared to PPLN and polymer waveguides, especially in the near-infrared spectral range. Our BPM waveguides have proved to be the most efficient, to our knowledge, both in terms of output powers observed and normalized efficiency. We have also demonstrated SHG in semiconductor waveguides for the first time using femtosecond pulses near 1.55 and 2.01 μm using MPM and BPM techniques, respectively. Our results confirm that these waveguides are highly promising for ultra-short pulse applications, including telecommunication applications. QPM waveguides also showed significant improvement in the observed SH power compared to our first demonstration and we strongly believe that there is scope for further enhancement in the output power. It should also be noted that the above experiments were all performed at room temperature and we did not observe any optical damage to the waveguides at any power level used and could easily couple $\sim$100 mW of 200 fs pulses without any sign of optical damage. The waveguides also remained chemically stable over a period of time of typically a few months with reproducible results. The field is still in its infancy and, as discussed above, the main challenges for these waveguides to be converted into practical devices are the optical losses, long-term stability and understanding of the spatial and temporal dynamics within the waveguide.

6. Conclusions

Semiconductor heterostructures based on GaAs offer attractive candidates for nonlinear frequency conversion in the near- and mid-infrared. Using the techniques of BPM, QPM and MPM, we have achieved phase matching in GaAs-based waveguides and demonstrated SHG at high efficiencies with practical output powers. Birefringent samples were found to be the most efficient among the samples investigated followed by MPM and QPM samples. The rapid progress from pW and nW output powers, in the initial stages of development of these techniques, to the μW and mW range at present is highly encouraging. Furthermore, a unique blend of theoretical modelling, materials processing, thorough characterization and investigation of device applications, providing an interactive feedback at different stages of fabrication and design for more effective optimization, will ensure GaAs-based compact optical sources (devices) in the very near future for a variety of applications. These include optical communications, WDM networks, frequency conversion, trace gas detection, chemical engineering and various other areas.

Acknowledgments

We are grateful to THALES, France, and the University of Glasgow, UK, for providing us with the samples used in these studies. We acknowledge the contributions, especially, from Professor V Berger and Dr A De Rossi of THALES and Dr A S Helmy, Dr K Zeaiter, Dr D C Hutchings and Professor J S Aitchison of the University of Glasgow. Most of the work presented here has been performed under the EU OFCORSE II project. We also acknowledge funding (grant no. GR/M78939) from EPSRC, UK.

Note added. After the final version of the manuscript was prepared two recent reports attracted our attention. One of them contained frequency conversion in periodically poled gallium nitride in the telecommunications window. Chowdhury *et al* [112] observed $\sim$9 μW of second-harmonic power from a fundamental input laser wavelength of 1658.6 nm with a normalized conversion efficiency of 12.76% W^{-1} cm^{-2}. The other paper [113] demonstrated quasi-phase-matched parametric fluorescence, essential for building an integrated OPO, in periodically sublattice-reversed gallium arsenide waveguides. These two reports vindicate our arguments that semiconductor waveguides are attractive for frequency conversion.

References

[1] Yoo S J B 1996 Wavelength conversion technologies for WDM network applications *IEEE J. Lightwave Technol.* **14** 955–66

[2] Campi D and Coriasso C 2000 Wavelength conversion technologies *Photon. Technol. Net.* **2** 85–95

[3] Popp A, Muller F, Kuhnemann F, Schiller S, von Basum G, Dahnke H, Hering P and Murtz M 2002 Ultra-sensitive mid-infrared cavity leak-out spectroscopy using a cw optical parametric oscillator *Appl. Phys.* B **75** 751–4

[4] Petrov K P, Ryan A T, Patterson T L, Huang L, Field S J and Bamford D J 1998 Spectroscopic detection of methane by use of guided-wave diode-pumped difference-frequency generation *Opt. Lett.* **23** 1052–4

[5] Chen W D, Burie J and Boucher D 1999 Mid-infrared generation by optical frequency conversion and applications to spectroscopy and air monitoring *Spectrochim. Acta* A **55** 2057–75

[6] Arie A, Fradkin-Kashi K and Shreberk Y 2002 Frequency conversion in novel materials and its application to high resolution gas sensing *Opt. Laser Eng.* **37** 159–70

[7] Lancaster D G, Richter D and Tittel F K 1999 Portable fiber-coupled diode-laser-based sensor for multiple trace gas detection *Appl. Phys.* B **69** 459–65

[8] Curl R F and Tittel F K 2002 Tunable infrared laser spectroscopy *Annu. Rep. Prog. Chem.* C **98** 217–70

[9] Kosterev A A, Tittel F K, Gmachl C, Capasso F, Sivco D L, Baillargeon J N, Hutchinson A L and Cho A Y 2000 Trace-gas detection in ambient air with a thermoelectrically cooled, pulsed quantum-cascade distributed feedback laser *Appl. Opt.* **39** 6866–72

[10] Richtera D, Erdelyia M, Curla R F, Tittel F K, Oppenheimer C, Duffell H J and Burton M 2002 Field measurements of volcanic gases using tunable diode laser based mid-infrared and Fourier transform infrared spectrometers *Opt. Laser Eng.* **37** 171–86

[11] Petrich W 2001 Mid-infrared and Raman spectroscopy for medical diagnostics *Appl. Spectrosc. Rev.* **36** 181–237

[12] de Barros M R X, Becker P C and Jedju T M 1996 Ultrafast mid-infrared pulse generation *Braz. J. Phys.* **26** 525–9

[13] Shoji I, Kondo T, Kitamoto A, Shirane M and Ito R 1997 Absolute scale of second-order nonlinear-optical coefficients *J. Opt. Soc. Am.* B **14** 2268–94

[14] Sutherland R L 1996 *Handbook of Nonlinear Optics* (New York: Dekker)

[15] van der Ziel J P 1975 Phase-matched harmonic generation in a laminar structure with wave propagation in the plane of the layers *Appl. Phys. Lett.* **26** 60–1

[16] Fiore A, Berger V, Rosencher E, Laurent N, Theilmann S, Vodjdani N and Nagle J 1996 Huge birefringence in selectively oxidized GaAs/AlAs optical waveguides *Appl. Phys. Lett.* **68** 1320–2

[17] Fiore A, Berger V, Rosencher E, Laurent N, Vodjdani N and Nagle J 1996 Birefringence phase matching in selectively oxidized GaAs/AlAs optical waveguides for nonlinear frequency conversion *J. Nonlinear Opt. Phys. Mater.* **5** 645–51

[18] Fiore A, Berger V, Rosencher E, Crouzy S, Laurent N and Nagle J 1997 $\Delta n = 0.22$ birefringence measurement by surface emitting second-harmonic generation in selectively oxidized GaAs/AlAs optical waveguides *Appl. Phys. Lett.* **71** 2587–9

[19] Fiore A, Berger V, Rosencher E, Bravetti P, Laurent N and Nagle J 1997 Phase-matched mid-infrared difference frequency generation in GaAs-based waveguides *Appl. Phys. Lett.* **71** 3622–4

[20] Fiore A, Berger V, Rosencher E, Bravetti P and Nagle J 1998 Phase-matching using an isotropic nonlinear optical material *Nature* **391** 463–6

[21] Fiore A, Janz S, Delobel L, van der Meer P, Bravetti P, Berger V, Rosencher E and Nagle J 1998 Second-harmonic generation at $\lambda = 1.6$ μm in $AlGaAs/Al_2O_3$ waveguides using birefringence phase matching *Appl. Phys. Lett.* **72** 2942–4

[22] Bravetti P, Fiore A, Berger V, Rosencher E, Nagle J and Gauthier-Lafaye O 1998 5.2–5.6 μm source tunable by frequency conversion in a GaAs-based waveguide *Opt. Lett.* **23** 331–3

[23] Leo G and Rosencher E 1998 Analysis of optically amplified mid-infrared parametric generation in AlGaAs waveguides *Opt. Lett.* **23** 1823–5

[24] Leo G, Berger V, OwYang C and Nagle J 1999 Parametric fluorescence in oxidized AlGaAs waveguides *J. Opt. Soc. Am.* B **16** 1597–602

[25] Moutzouris K, Venugopal Rao S, Ebrahimzadeh M, De Rossi A, Berger V, Calligaro M and Ortiz V 2001 Efficient second-harmonic generation in GaAs/AlGaAs waveguides using birefringent phase matching *Opt. Lett.* **26** 1785–7

[26] De Rossi A, Berger V, Calligaro M, Leo G, Ortiz V and Marcadet X 2001 Parametric fluorescence in oxidized aluminum gallium arsenide waveguides *Appl. Phys. Lett.* **79** 3758–60

[27] de Sande J C G, Leo G and Assanto G 2002 Phase-matching engineering in birefringent AlGaAs waveguides for difference frequency conversion *J. Lightwave Technol.* **20** 651–60

[28] Leo G, Assanto G, Durand O and Berger V 2002 Characterization of AlGaAs/AlAs waveguides for optical parametric interactions *J. Opt. Soc. Am.* B **19** 902–10

[29] Rosencher E 2000 Towards integrated semiconductor optical parametric oscillators *C. R. Acad. Sci.* IV **1** 615–25

[30] De Rossi A, Calligaro M, Ortiz V and Berger V 2002 Towards an optical parametric oscillator in a GaAs-based waveguide *OSA Digest on Nonlinear Guided Waves and Their Applications* NLMD42

[31] Janz S, Fernando C, Dai H, Chatenoud F and Normandin R 1993 Quasi-phase-matched second-harmonic generation in reflection from $Al_xGa_{1-x}As$ heterostructures *Opt. Lett.* **18** 589–91

[32] Yoo S J B, Bhat R, Caneau C and Koza M A 1995 Quasi-phase-matched second-harmonic generation in AlGaAs waveguides with periodic domain inversion achieved by wafer bonding *Appl. Phys. Lett.* **66** 3410–2

[33] Yoo S J B, Caneau C, Bhat R, Koza M A, Rajhel A and Antoniades N 1996 Wavelength conversion by difference frequency generation in AlGaAs waveguides with periodic domain inversion achieved by wafer bonding *Appl. Phys. Lett.* **68** 2609–11

[34] Janz S, Beaulieu Y, Fiore A, Bravetti P, Berger V, Rosencher E and Nagle J 1997 Surface emitted second-harmonic generation from a quasi-phase matched waveguide in an $Al_xGa_{1-x}As/Al_2O_3$ microcavity *Opt. Express* **2** 462–70

[35] Fiore A, Beaulieu Y, Janz S, McCaffrey J P, Wasilewski Z R and Xu D X 1997 Quasiphase matched surface emitting second-harmonic generation in periodically reversed asymmetric GaAs/AlGaAs quantum well waveguide *Appl. Phys. Lett.* **70** 2655–7

[36] Janz S, Buchanan M, van der Meer P, Wasilewski Z R, Xu D-X, Piva P, Mitchell I V, Akano U G and Fiore A 1998 Patterning the second-order optical nonlinearity of asymmetric quantum wells by ion implantation enhanced intermixing *Appl. Phys. Lett.* **72** 3097–9

[37] Hamilton C J, Marsh J H, Hutchings D C, Aitchison J S, Kennedy G T and Sibbett W 1996 Localized Kerr-type nonlinearities in GaAs/AlGaAs multiple quantum well structures at 1.55 μm *Appl. Phys. Lett.* **68** 3078–80

[38] Street M W, Whitbread N D, Hamilton C J, Vögele B, Stanley C R, Hutchings D C, Marsh J H, Aitchison J S, Kennedy G T and Sibbett W 1997 Modification of the second-order optical nonlinearities in AlGaAs asymmetric multiple quantum well waveguides by quantum well intermixing *Appl. Phys. Lett.* **70** 2804–6

[39] Street M W, Whitbread N D, Hutchings D C, Arnold J M, Marsh J H, Aitchison J S, Kennedy G T and Sibbett W 1997 Quantum-well intermixing for the control of the second-order nonlinear effects in AlGaAs multiple-quantum-well waveguides *Opt. Lett.* **22** 1600–2

[40] Hutchings D C and Arnold J M 1997 Determination of second-order nonlinear coefficients in semiconductors using pseudospin equations for three-level systems *Phys. Rev.* B **56** 4056–67

[41] Aitchison J S, Street M W, Whitbread N D, Hutchings D C, Marsh J H, Kennedy G T and Sibbett W 1998 Modulation of the second-order nonlinear tensor components in multiple-quantum-well structures *IEEE J. Sel. Top. Quantum Electron.* **4** 695–700

[42] Hutchings D C 2000 Modulation of the second-order susceptibility in GaAs/AlAs superlattices *Appl. Phys. Lett.* **76** 1362–4

[43] Helmy A S, Hutchings D C, Kleckner T C, Marsh J H, Bryce A C, Arnold J M, Stanley C R, Aitchison J S, Brown C T A, Moutzouris K and Ebrahimzadeh M 2000 Quasi-phase matching in GaAs–AlAs superlattice waveguides through bandgap tuning by use of quantum-well intermixing *Opt. Lett.* **25** 1370–3

[44] Bouchard J-P, Tetu M, Janz S, Xu D-X, Wasilewski Z R, Piva P, Akano U G and Mitchell I V 2000 Quasi-phase matched second-harmonic generation in an $Al_xGa_{1-x}As$ asymmetric quantum-well waveguide using ion-implantation-enhanced intermixing *Appl. Phys. Lett.* **77** 4247–9

[45] Hutchings D C and Kleckner T C 2002 Quasi-phase matching in semiconductor waveguides by intermixing: optimization considerations *J. Opt. Soc. Am.* B **19** 890–4

[46] Zeaiter K, Hutchings D C, Gwilliam R M, Moutzouris K, Venugopal Rao S and Ebrahimzadeh M 2003 Quasi-phase matched second-harmonic generation in GaAs/AlAs superlattice waveguide using ion-implantation induced intermixing *Opt. Lett.* **28** 911–3

[47] Anderson D B and Boyd J T 1971 Wideband CO_2 laser second-harmonic generation phase matched in GaAs thin-film waveguides *Appl. Phys. Lett.* **19** 266–8

[48] van der Ziel J P, Miller R C, Logan R A, Nordland W A Jr and Mikulyak R M 1974 Phase-matched second-harmonic generation in GaAs optical waveguides by focused laser beam *Appl. Phys. Lett.* **25** 238–40

[49] Chowdhury A and McCaughan L 2000 Continuously phase-matched M-waveguides for second-order nonlinear upconversion *IEEE Photon. Technol. Lett.* **12** 486–8

[50] Oster B and Fouckhardt H 2001 Variations of optical M-waveguides for direct phase matching in AlGaAs *IEEE Photon. Technol. Lett.* **13** 672–4

[51] Oster B and Fouckhardt H 2001 M-waveguide structures for direct phase matching in AlGaAs *Appl. Phys.* B **73** 535–40

[52] Moutzouris K, Venugopal Rao S, Ebrahimzadeh M, De Rossi A, Calligaro M, Ortiz V and Berger V 2003 Femtosecond second-harmonic generation through optimized modal phase matching in semiconductor waveguides *Appl. Phys. Lett.* **83** 620–2

[53] Rafailov E U, Alvarez P L, Brown C T A, Sibbett W, De La Rue R M, Millar P, Yanson D A, Roberts J S and Houston P A 2001 Second-harmonic generation from a first-order quasi-phase-matched GaAs/AlGaAs waveguide crystal *Opt. Lett.* **26** 1984–6

[54] Rafailov E U, Loza-Alvarez P, Artigas D, Flynn M B and Sibbett W 2002 Novel type semiconductor waveguide crystal for efficient frequency up/down conversion *OSA Digest on Nonlinear Guided Waves and Their Applications* NLMD5-1

[55] Koh S, Kondo T, Shiraka Y and Ito R 2001 GaAs/Ge/GaAs sublattice reversal epitaxy and its application to nonlinear optical devices *J. Cryst. Growth* **227/228** 183–92

[56] Xu C-Q, Takemasa K, Nakamura K, Wada H, Takamori T, Okayama H and Kamijoh T 1996 Confirmation of AlGaAs crystal domain inversion using asymmetric wet etching and optical second-harmonic generation methods *Japan. J. Appl. Phys.* **35** L1419–21

[57] Xu C Q, Takemasa K, Nakamura K, Okayama H and Kamihoh T 1998 AlGaAs semiconductor quasi-phase-matched wavelength converters *Japan. J. Appl. Phys.* **37** 823–31

[58] Skauli T, Vodopyanov K L, Pinguet T J, Schober A, Levi O, Eyres L A, Fejer M M, Harris J S, Gerard B, Becouarn L, Lallier E and Arisholm G 2002 Measurement of the nonlinear coefficient of orientation-patterned GaAs and demonstration of highly efficient second-harmonic generation *Opt. Lett.* **27** 628–30

[59] Yu X, Scaccabarozzi L, Levi O, Pinguet T J, Fejer M M and Harris J S Jr 2003 Template design and fabrication for low-loss orientation-patterned nonlinear AlGaAs waveguides pumped at 1.55 μm *J. Cryst. Growth* **251** 794–9

[60] Ebert C B, Eyres L A, Fejer M M and Harris J S Jr 1999 MBE growth of antiphase GaAs films using GaAs/Ge/GaAs heteroepitaxy *J. Cryst. Growth* **201/202** 187–93

[61] Eyres L A, Tourreau P J, Pinguet T J, Ebert C B, Harris J S, Fejer M M, Becouarn L, Gerard B and Lallier E 2001 All-epitaxial fabrication of thick, orientation-patterned GaAs films for nonlinear optical frequency conversion *Appl. Phys. Lett.* **79** 904–6

[62] Gordon L, Woods G L, Eckardt R C, Route R R, Feigelson R S, Fejer M M and Byer R L 1994 Diffusion-bonded stacked GaAs for quasi-phase-matched second-harmonic generation of a carbon dioxide laser *Electron. Lett.* **29** 1942–4

[63] Lallier E, Brévignon M and Lehoux J 1998 Efficient second-harmonic generation of a CO_2 laser with a quasi-phase-matched GaAs crystal *Opt. Lett.* **23** 1511–3

[64] Lallier E, Becouarn L, Brévignon M and Lehoux J 1998 Infrared difference frequency generation with quasi-phase-matched GaAs *Electron. Lett.* **34** 1609–10

[65] Becouarn L, Gerard B, Brévignon M, Lehoux J, Ggourdel Y and Lallier E 1998 Second-harmonic generation of CO_2 laser using thick quasi-phase-matched GaAs layer grown by hydride vapour phase epitaxy *Electron. Lett.* **34** 2409–10

[66] Ueno Y, Ricci V and Stegeman G I 1997 Second-order susceptibility of $Ga_{0.5}In_{0.5}P$ crystals at 1.5 μm and their feasibility for waveguide quasi-phase matching *J. Opt. Soc. Am.* B **14** 1428–36

[67] Rustagi K C, Mehendale S C and Meenakshi S 1982 Optical frequency conversion in quasi-phase matched stacks of nonlinear crystals *IEEE J. Quantum Electron.* **18** 1029–41

[68] Xu C Q, Okayama H and Kawahara M 1995 Optical frequency conversions in nonlinear medium with periodically modulated linear and nonlinear optical parameters *IEEE J. Quantum Electron.* **31** 981–7

[69] Lim E J, Hertz H M, Bortz M L and Fejer M M 1991 Infrared radiation generated by quasi-phase-matched difference-frequency mixing in a periodically poled lithium niobate waveguide *Appl. Phys. Lett.* **59** 2207–9

[70] Fejer M M, Magel G A, Jundt D H and Byer R L 1992 Quasi-phase-matched second harmonic generation: tuning and tolerances *IEEE J. Quantum Electron.* **28** 2631–54

[71] Bortz M L, Arbore M A and Fejer M M 1995 Quasi-phase-matched optical parametric amplification and oscillation in periodically poled $LiNbO_3$ waveguides *Opt. Lett.* **20** 49–51

[72] Arbore M A and Fejer M M 1997 Singly resonant optical parametric oscillation in periodically poled lithium niobate waveguides *Opt. Lett.* **22** 151–3

[73] Parameswaran K R, Kurz J R, Rostislav R V, Roussev V and Fejer M M 2002 Observation of 99% pump depletion in single-pass second-harmonic generation in a periodically poled lithium niobate waveguide *Opt. Lett.* **27** 43–5

[74] Parameswaran K R, Route R K, Kurz J R, Roussev R V, Fejer M M and Fujimara M 2002 Highly efficient second-harmonic generation in buried waveguides formed by annealed and reverse proton exchange in periodically poled lithium niobate *Opt. Lett.* **27** 179–81

[75] Zheng Z, Weiner A M, Parameswaran K R, Chou M-H and Fejer M M 2002 Femtosecond second-harmonic generation in periodically poled lithium niobate waveguides with simultaneous strong pump depletion and group-velocity walk-off *J. Opt. Soc. Am.* B **19** 839–48

[76] Stegeman G I and Seaton C T 1985 Nonlinear integrated optics *J. Appl. Phys.* **58** R57–77

[77] Stegeman G I and Stolen R H 1989 Waveguides and fibers for nonlinear optics *J. Opt. Soc. Am.* B **6** 652–62

[78] Stegeman G I 1992 Introduction to nonlinear guided wave optics *Guided Wave Nonlinear Optics* ed D B Ostrowsky and R Reinisch (Dordrecht: Kluwer–Academic) pp 11–27

[79] Jäger M, Stegeman G I, Flipse M C, Diemeer M and Möhlmann G 1996 Modal dispersion phase matching over 7 mm length in over damped polymeric channel waveguides *Appl. Phys. Lett.* **69** 4139–41

[80] Jäger M, Stegeman G I, Möhlmann G R, Flipse M C and Diemeer M B J 1996 Second-harmonic generation in

polymeric channel waveguides using modal dispersion *Electron. Lett.* **32** 2009–10

[81] Wirges W, Yilmaz S, Brinker W, Bauer-Gogonea S, Bauer S, Jäger M, Stegeman G I, Ahlheim M, Stähelin M, Zysset B, Lehr F, Diemeer M and Flipse M C 1997 Polymer waveguides with optimized overlap integral for modal dispersion phase-matching *Appl. Phys. Lett.* **70** 3347–9

[82] Jäger M, Stegeman G I, Brinker W, Yilmaz S, Bauer S, Horsthuis W H G and Mohlmann G R 1996 Comparison of quasi-phase-matching geometries for second-harmonic generation in poled polymer channel waveguides at 1.5 μm *Appl. Phys. Lett.* **68** 1183–5

[83a] Dai T, Singer K D, Twieg R J and Kowalczyk T C 2000 Anomalous-dispersion phase-matched second-harmonic generation in polymer waveguides: chromophores for increased efficiency and ultraviolet stability *J. Opt. Soc. Am.* B **17** 412–21

[83b] Martin G, Ducci S, Hierle R, Josse D and Zyss J 2003 Quasiphase matched second-harmonic generation from periodic optical randomization of poled polymer channel waveguides *Appl. Phys. Lett.* **83** 1086–8

[84] Canva M and Stegeman G I 2002 Quadratic parametric interactions in organic waveguides *Advances in Polymer Science* vol 158 (Berlin: Springer) pp 87–121

[85] Phillips P J, Das S and Ebrahimzadeh M 2000 High-repetition-rate, all-solid-state, Ti:sapphire-pumped optical parametric oscillator for the mid-infrared *Appl. Phys. Lett.* **77** 469–71

[86] Venugopal Rao S, Moutzouris K, Ebrahimzadeh M, De Rossi A, Calligaro M, Ortiz V, Ginitz G and Berger V 2002 Measurements of optical loss in GaAs/Al_2O_3 nonlinear waveguides in the infrared using femtosecond scattering technique *Opt. Commun.* **213** 223–8

[87] Venugopal Rao S, Moutzouris K, Ebrahimzadeh M, De Rossi A, Calligaro M, Ortiz V, Ginitz G and Berger V 2003 Influence of two-photon absorption and scattering on the optical loss in GaAs/Al_2O_3 nonlinear waveguides using femtosecond pulses *IEEE J. Quantum Electron.* **39** 478–86

[88] For example, see Li E H, Koteles E S and Marsh J H (ed) 1998 *IEEE J. Sel. Top. Quantum Electron.* **4** 581–803 (Special issue: Interdiffused Quantum-Well Materials and Devices)

[89] Kowalski O P, Hamilton C J, McDougall S D, Marsh J H, Bryce A C, De la Rue R M, Vogele B, Stanley C R, Button C C and Roberts J S 1997 A universal damage induced technique for quantum well intermixing *Appl. Phys. Lett.* **72** 581–3

[90] McDougall S D, Kowalski O P, Hamilton C J, Camacho F, Qiu B, Ke M, De la Rue R M, Bryce A C and Marsh J H 1998 Monolithic integration via a universal damage enhanced quantum-well intermixing technique *IEEE Sel. Top. Quantum Electron.* **4** 636–46

[91] Leier H, Forchel A, Horcher G, Hommel J, Bayer S, Rothfritz H, Weimann G and Schlapp W 1990 Mass and dose dependence of ion-implantation-induced intermixing of GaAs GaAlAs quantum-well structures *J. Appl. Phys.* **67** 1805–13

[92] Kleckner T C 2002 Quasi-phase-matched nonlinear frequency conversion in periodically disordered GaAs/AlAs superlattice-core waveguides *PhD Thesis* University of Glasgow

[93] De Angelis C, Gringoli F, Midrio M, Modotto D, Aitchison J S and Nalesso G F 2001 Conversion efficiency for second-harmonic generation in photonic crystals *J. Opt. Soc. Am.* B **18** 348–51

[94] Modotto D 2002 private communication

[95] Kowalczyk T C, Singer K D and Cahill P A 1995 Anomalous-dispersion phase-matched second-harmonic generation in a polymer waveguide *Opt. Lett.* **15** 2273–5

[96] Sugihara O, Kinoshita T, Okabe M, Kunioka S, Nanoka Y and Sasaki K 1991 Phase-matched second-harmonic generation in poled dye/polymer waveguide *Appl. Opt.* **30** 2957–60

[97] Clays K, Schildkraut J S and Williams D J 1994 Phase-matched second-harmonic generation in a four-layered polymeric waveguide *J. Opt. Soc. Am.* B **11** 655–64

[98] Wagner H P, Whittmann S, Schmitzer H and Stanzl H 1995 Phase matched second-harmonic generation using thin ZnTe optical waveguides *J. Appl. Phys.* **77** 3637–40

[99] Khalil M A, Vitrant G, Raimond P, Chollet P A and Kajzar F 1999 Modal dispersion phase-matched frequency doubling in composite planar waveguide using ion-exchanged glass and optically nonlinear poled polymer *Opt. Commun.* **170** 281–4

[100] Flueraru C and Grover C P 2003 Overlap integral analysis for second-harmonic generation within inverted waveguide using mode dispersion phase match *IEEE Photon. Technol. Lett.* **15** 697–9

[101] De Rossi A and Berger V 2000 *International Workshop on Quantum Information (Postdam, Sept. 2000)* First annual report, Project IST-1999-10033 QUCOMM

[102] De Rossi A, Semaltianos N, Chiralis E, Vinter B, Ortiz V and Berger V 2002 Third order mode optically pumped semiconductor laser *Appl. Phys. Lett.* **80** 4690–2

[103] Herzinger C M, Lu C-C, De Temple T A and Chew W C 1993 The semiconductor waveguide facet reflectivity problem *IEEE J. Quantum Electron.* **29** 2273–81

[104] Hofmann D, Schreiber G, Haase C, Hermann H, Grundkötter W, Ricken R and Sohler W 1999 Quasi-phase-matched difference-frequency generation in periodically poled Ti:$LiNbO_3$ channel waveguides *Opt. Lett.* **24** 896–8

[105] Mizuuchi K, Ohta H, Yamamoto K and Kato M 1997 Second-harmonic generation with a high-index-clad waveguide *Opt. Lett.* **22** 1217–9

[106] Mizuuchi K and Yamamoto K 1998 Waveguide second-harmonic generation device with broadened flat quasi-phase-matching response by use of a grating structure with located phase shifts *Opt. Lett.* **23** 1880–2

[107] Yamamoto K, Mizuuchi K, Kitoaka Y and Kato M 1995 Highly efficient quasi-phase-matched second-harmonic generation by frequency doubling of a high-frequency superimposed diode laser *Opt. Lett.* **20** 273–5

[108a] Sugita T, Mizuuchi K, Kitaoka Y and Yamamoto K 2001 Ultraviolet light generation in a periodically poled MgO:$LiNbO_3$ waveguide *Japan. J. Appl. Phys.* **40** 1751–3

[108b] Mizuuchi K, Sugita T, Yamamoto K, Kawaguchi T, Yoshino T and Imaeda M 2003 Efficient 340 nm light generation by a ridge-type waveguide in a first-order periodically poled MgO:$LiNbO_3$ *Opt. Lett.* **28** 1344–6

[109] Sato D, Morita T, Suhara T and Fujimara M 2003 Efficiency improvement by high-index cladding in $LiNbO_3$ waveguide quasi-phase-matched wavelength converter for optical communication *IEEE Photon. Technol. Lett.* **15** 569–71

[110] Zhou B, Xu C-Q and Chen B 2003 Comparison of difference frequency generation and cascaded $\chi^{(2)}$ based wavelength conversions in $LiNbO_3$ quasi-phase-matched waveguides *J. Opt. Soc. Am.* B **20** 846–52

[111] Webjörn J, Siala S, Nam D W, Waarts R G and Lang R J 1997 Visible laser sources based on frequency doubling in nonlinear waveguide *IEEE J. Quantum Electron.* **33** 1673–86

[112] Chowdhury A, Ng H M, Bhardwaj M and Weimann N G 2003 Second-harmonic generation in periodically poled GaN *Appl. Phys. Lett.* **83** 1077–9

[113] Tachibana H, Matsushita T, Ara K and Kondo T 2003 Quasi-phase-matched parametric fluorescence in periodically inverted GaAs waveguides *CMA6: Proc. CLEO (Baltimore, USA, 2003)*